Optical Materials 133 (2022) 112905

Contents lists available at ScienceDirect

Optical Materials

journal homepage: www.elsevier.com/locate/optmat

Research Article

Investigation of TiO_2 and Ce^{3+}-activated TiO_2 particles on optical properties of the PMMA embedded YAG: Ce^{3+} and LuAG: Ce^{3+}

Beyza Yildirim [a], Ozgur Yasin Keskin [b,c], Ramazan Dalmis [c], Isil Birlik [c], Funda Ak Azem [c], Kadriye Ertekin [d,e,*]

[a] Dokuz Eylul University, The Graduate School of Natural and Applied Sciences, Department of Chemistry, Buca, 35390, Izmir, Turkey
[b] Dokuz Eylul University, The Graduate School of Natural and Applied Sciences, Department of Metallurgical and Materials Engineering, Buca, 35390, Izmir, Turkey
[c] Dokuz Eylul University, Department of Metallurgical and Materials Engineering, Buca, 35390, Izmir, Turkey
[d] Dokuz Eylul University, Department of Chemistry, Faculty of Science, Buca, 35390, Izmir, Turkey
[e] Dokuz Eylul University, Center for Fabrication and Applications of Electronic Materials (EMUM), Buca, 35390, Izmir, Turkey

ARTICLE INFO

Keywords:
LuAG
Ce^{3+}
YAG
TiO_2
Fluorescence
Photoluminescence
Decay time

ABSTRACT

Ce^{3+} activated garnets; LuAG and YAG are extensively used in lighting applications, electronics, and display technologies. Both of the phosphors have been studied many times to increase their brightness and provide a red-shift in their emission maximum towards warmer colors for potential white light emitting diode (WLED) applications. In this work, binary blends of the LuAG: Ce^{3+} with the micro-scale TiO_2 and Ce^{3+}-equipped TiO_2 particles were prepared and tested in terms of photoluminescence characteristics in a polymethyl methacrylate (PMMA) matrix. Similar work was also performed for the YAG: $Ce^{3+}$and its TiO_2-based composites. Blue-wavelength excitation and emission performances as well as decay characteristics of the phosphors were investigated in detail. When excited by blue wavelengths, the TiO_2 blends of the LuAG: Ce^{3+} and YAG: Ce^{3+} exhibited strong enhancement in emission intensities extending to 2.80 and 2.20 fold in comparison to their additive-free forms. Additionally, 32 and 66 nm of red shifts were measured in the emission maximum of the TiO_2-based blends, respectively. The decay time measurements performed in the microsecond time scale revealed parallel variations to the increases observed in the intensities. The distinguishable enhancement observed in the quantum efficiency of the phosphors by using cost-effective TiO_2 particles can be concluded as a remarkable development. Additionally, the ability of the phosphor blends to be excited with simple blue LEDs looks very promising for future lighting applications.

1. Introduction

Intensive studies on the synthesis and development of the cerium-activated yttrium and lutetium aluminum garnets ((YAG: Ce^{3+}) and (LuAG: Ce^{3+})) continue due to their potential utilization in the fabrication of white light-emitting diodes (WLEDs), efficient scintillation processes in the detection of X and gamma-rays, solid-state lasers and many other applications [1–5]. The widespread usage of the Ce^{3+} doped YAG and LuAG as complementary phosphors in different matrices in the production of WLEDs increased their commercial importance and consequently the number of related patent applications over time [6–12]. Most of these studies focus on compositional modifications on the YAG or LuAG-based garnets to improve the optical performance of the subjective materials via the utilization of expensive rare earths as dopants or co-dopants [12–26]. In most of these studies, donor and acceptor counterparts have been used to form appropriate energy levels within the lattice for a potential energy transfer and a consequent optical brightness [16,19–21]. Sometimes these efforts resulted in variations in the size or structure of the lattice including increased defects or electron traps to capture the electrons [2,17,18,25]. However, the introduction of these rare earths into the lattice structure requires tedious thermal processes and high temperatures extending to 1500 °C requiring an inert gas atmosphere [2,13–15]. A summary of the synthetic efforts including compositional studies and energy transfer agents used in the YAG and LuAG-based phosphors has been shown in Table 1.

Contrary to the studies using expensive REs as dopants or co-dopant in the lattice structure, in recent years, Hu et al. offered a different strategy to fabricate a high-quality YAG: Ce^{3+} material for laser-diode

* Corresponding author. Dokuz Eylul University, Department of Chemistry, Faculty of Science, Buca, 35390, Izmir, Turkey.
E-mail address: kadriye.ertekin@deu.edu.tr (K. Ertekin).

https://doi.org/10.1016/j.optmat.2022.112905
Received 4 June 2022; Received in revised form 30 July 2022; Accepted 17 August 2022
0925-3467/© 2022 Published by Elsevier B.V.

Table 1
Literature research on synthetic efforts and compositional studies on the YAG and LuAG-based phosphors.

Phosphor	Dopant/ Co-dopant	Mechanism	Result
YAG	Ce/Sm	Energy transfer from Ce to Sm	Enhancing the color quality of white light emitting diodes [16].
	Ce^{3+}/ Eu^{3+}	Increased defects	Red shift of the PL emission band [17].
	Ce^{3+}/ Sr^{2+}	Increased defects	A significant enhancement in photoluminescence excitation and emission spectra [2]
	Ce^{3+}/ Cr^{3+}	Volume effect	Brighter persistent luminescence [18]
	Nd3+/ Yb3+	Energy transfer occurs from Nd^{3+} to Yb^{3+}.	A predominant electric dipole–dipole character for the Nd3+–Yb3+ coupling is taking place [19].
	Tb^{3+}/ Cr^{3+}	Tb^{3+} to Cr^{3+} energy transfer	External quantum efficiency was increased up to 98% [20]
LuAG	Ce/Mn	Energy transfer from Ce^{3+} to Mn^{2+} (up to 42.3%)	The emitted light changed from green to orange [21].
	Mg^{2+}/ Ce^{4+}	Compensation of oxygen vacancies, stimulation of cerium into 4+ charge state, and localization of O-hole centers nearby the Mg^{2+} dopant	An increase in scintillation light yield (LY) value [22].
	Tm/Sc	Energy transfer	Scintillation yield was enhanced [23].
	Ce^{3+}/ Tb^{3+}	Energy transfer from Tb^{3+} to Ce^{3+}	Co-doping with Tb^{3+} does not result in the desired increase in light output [24].
	Ce^{3+}/ Ca^{2+}	Ca^{2+} and Ce^{3+} were partially oxidized to Ce^{4+}, which can effectively compete with electron traps to capture electrons.	A significant improvement in the scintillation performance [25].
	Sc^{3+}/ Pr^{3+}	Energy transfer from sensitizer Sc^{3+} to activator Pr^{3+}	Increased radioluminescence intensity and photoelectron yield [26].

(LD) lighting applications. They proposed to depress the defects by using the charge-balanced Mg^{2+}-Si^{4+} to substitute the Al^{3+}-Al^{3+} by introducing Al_2O_3 into the structure of the garnet [27]. In another work, Gu and colloquies studied the effect of boron carbide (B_4C) on luminescent efficiency and thermal stability of $Y_3Al_5O_{12}$:Ce^{3+} phosphors. By the incorporation of the B^{3+} ions, they obtained a red-shifted emission, a distinct improvement in the luminescent efficiency, and enhanced thermal stability for the YAG: Ce^{3+} phosphor [15]. Similarly, Yan and co-workers designed an energy transfer from Eu^{3+} to Mn^{4+} in the $Lu_3Al_5O_{12}$ (LuAG) garnet host. In this way, they tuned the photoluminescence from the narrow orange-red emission region (593 nm) to narrow deep-red light (668 nm), successfully [28]. Huang and co-workers presented ceramics containing Cr: YAG/Ce: YAG and (Ce, Cr): YAG/Ce: YAG with high color rendering index for white LED and LD applications [29]. In another study, researchers proposed doping of the heavy Ce^{3+} above the solid solubility limit into the LuAG host lattice to achieve a significant red-shift without Y and Gd ions, matching the yellow emission spectrum of commercial yellow YAG: Ce^{3+} [30]. Despite the promising spectral results, the existing technology mainly relays on structural changes in phosphors, which is laborious and costly. The design of an energy transfer between a number of luminescent centers within the lattice is an efficient strategy to provide the desired optical brightness. Alternatively, providing the fundamental conditions of a simple energy transfer between the lattice and its microenvironment may be an efficient way to improve the excitation efficiency and brightness of the phosphor. Today, there is a large number of micro- and or nano-scale light harvesting optically responsive materials that can be considered functional and cost-effective. In this context, the utilization of this type of material along with the phosphors in the polymeric matrices is worthy of studying. Preliminary studies have shown that the preparation of binary or ternary mixtures of phosphors with the light-harvesting metal oxides reveals promising results. The target-specific materials investigated by our research group include nano-scale ZnO–CuO particles [31], silica photonic crystals [32], and hematite (HEM) and iodine-decorated hematite (I-HEM) [33]. Therefore, in this work, we studied the light-induced interactions taking place in the binary blends of commercially available YAG: Ce^{3+}-and lab-synthesized TiO_2, and, TiO_2: Ce^{3+} in the polymethylmethacrylate (PMMA) matrix, in terms of the excitation-emission characteristics as well as decay times. The PMMA was chosen due to its resistance to heat, UV radiation, biocompatibility, and tailoring ability in many different structural forms. It is also preferred due to its good dispersant properties for high-density phosphors [34] as well as evidenced appropriate optical transparency in the visible and IR spectral region [35, 36].

The lutetium aluminum garnet (LuAG: Ce^{3+}) and yttrium aluminum garnet (YAG: Ce^{3+}) were entrapped along with the micro-scale Ce^{3+}-free and -Ce^{3+} doped TiO_2 particles, which can act as light-harvesting materials absorbing and emitting the light in a quite large spectrum. We excited the phosphors with the blue wavelengths (450 and 466 nm) which corresponds to the commonly used excitation energy for LED applications. Upon excitation, the phosphors exhibited interesting interactions with the micro-scale TiO_2 particles yielding enhanced quantum yield and longer excited-state lifetimes compared to their additive-free forms. We also investigated the decay characteristics of the presented composites in nanosecond and microsecond time scales in detail. In nanosecond time-regime measurements, the polymer-free and polymer-embedded YAG: Ce^{3+}, LuAG: Ce^{3+} and their binary blends with the additives exhibited typical average decay time of the bare phosphors arising from the electronic transitions of the Ce^{3+} ions which appeared around 50–60 ns. However, the multi-exponential microsecond time-regime measurements supported the donor-acceptor relationship for the additives and the phosphors, respectively. Average excited-state lifetime of the LuAG: Ce^{3+} extended from 379 to 522 μs when blended with the TiO_2:Ce^{3+}. The decay time was found to be 561 μs for the Ce^{3+}-free TiO_2-based composites. Similarly, the excited state lifetime of the YAG: Ce^{3+} increased from 268 to 407 and 417 μs, for the TiO_2:Ce^{3+} and TiO_2 including composite films, respectively.

2. Experimental

2.1. Materials

The precursors of the TiO_2-based oxides; Titanium (IV) isopropoxide (TTIP) and Cerium (III) chloride hexahydrate were purchased from Sigma Aldrich and Merck, respectively. Glacial acetic acid (Merck) and anhydrous ethanol (Sigma Aldrich) were used for the sol-gel preparation of the particles. Polymethylmethacrylate (PMMA) and Tetrahydrofuran (THF ≥99) were from Sigma Aldrich. The green and yellow phosphors; $Lu_3Al_5O_{12}$:Ce^{3+} (LuAG) and ($Y_3Al_5O_{12}$:Ce^{3+} (YAG) were provided by Mitsubishi Chemical Corporation. Ce^{3+}-free and Ce^{3+} doped TiO_2 particles were synthesized by the sol-gel method in our laboratories. Preparation protocols, XPS analysis, and reflectance behavior of the TiO_2 and TiO_2:Ce^{3+} particles were shown in the supplementary files (See S1 and S2).

2.2. Instrumentation

Excitation and emission spectra of the phosphors were recorded by an Edinburgh Instruments; FLS920 spectrometer in the steady-state mode. The incident light spectrum (the emission spectrum of the excitation light scattered by a BaSO4 as reflectance standard) and sample

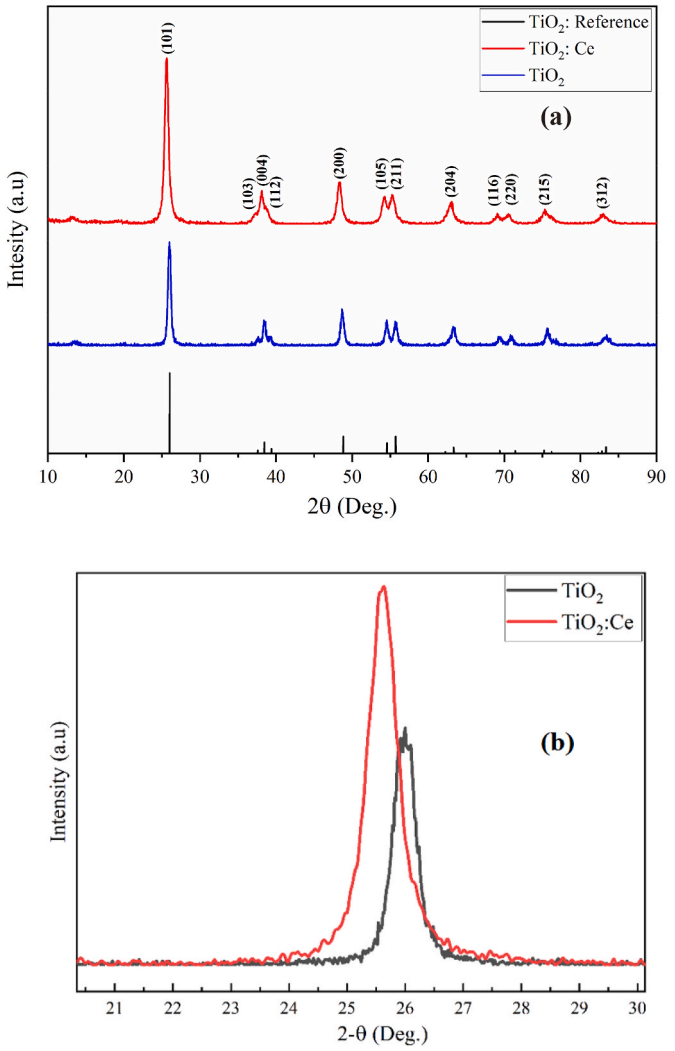


Fig. 1. (a) General and (b) overlaid XRD patterns of the TiO_2 and TiO_2:Ce^{3+} particles.

spectrum were recorded by the FLS920 Fluorescence Spectrometer equipped with a 150 W Xe lamp and an integrating sphere, respectively. The external quantum yield (EQY) data were acquired by adjusting the excitation wavelength in the 270–500 nm range. The decay times were recorded on the bases of the time-correlated single-photon counting (TCSPC) approach under the excitation of a pulsed laser and a microsecond flash lamp, for the nanosecond and microsecond time scales, respectively. The excitation and emission slits were adjusted to 1.5 or 5.0 nm. The Instrument Response Function (IRF) was recorded via a suspension of colloidal silica in water (LUDOX 30%, Sigma Aldrich). The UV-VIS spectral data of the samples were acquired by a Thermo-Scientific Evolution 600 Instrument. Crystal structures of the particles were investigated with an X-ray diffractometer instrument (XRD) using Rigaku D/Max-2200/PC diffractometer with a Cu Kα radiation source (λ = 0.1542 nm) working at 40 kV and under 30 mA of current, over 2θ range of 3–90°.

The XPS analysis of the phosphors and TiO2-based forms was performed with a Thermo-Scientific instrument equipped with an Al-K_α source. Particle morphologies, zeta potential measurements, and sizes of the samples were clarified by a Zeiss Sigma 500 field emission scanning electron microscope, and, the Malvern Zetasizer Nano ZS model device, respectively.

Table 2
Composition of the luminescent materials.

Sample	Phosphor: 10 mg	Additive: 10 mg	Matrix: 120 mg	Solvent: 2 mL
LuAG:Ce^{3+}	LuAG:Ce^{3+}	–	PMMA	THF
LuAG:Ce^{3+} - TiO_2	LuAG:Ce^{3+}	TiO_2	PMMA	THF
LuAG:Ce^{3+}- TiO_2:Ce^{3+}	LuAG:Ce^{3+}	TiO_2:Ce^{3+}	PMMA	THF
YAG:Ce^{3+}	YAG:Ce^{3+}	–	PMMA	THF
YAG:Ce^{3+} - TiO_2	YAG:Ce^{3+}	TiO_2	PMMA	THF
YAG:Ce^{3+} - TiO_2:Ce^{3+}	YAG:Ce^{3+}	TiO_2:Ce^{3+}	PMMA	THF

3. Results and discussions

3.1. X-ray diffraction analysis of the TiO_2 and TiO_2:Ce^{3+} particles

Fig. 1 (a) shows XRD patterns of Ce^{3+}-free and Ce^{3+}-doped TiO_2 particles, respectively. The diffraction peaks located at 25.2°, 37.8°, 48.0°, 53.9°, 55.1°, 62.7°, 68.8°, 70.3°, 74.0°, and 76.1° tagged with Miller indices of (101), (004), (200), (105), (211), (204), (116), (220), (107), and (301), well match with the main peaks of the anatase phase (JCPDS card No. 21–1272) respectively. Both, the **TiO_2 and TiO_2:Ce^{3+}** exhibited good crystalline structure indicating the anatase phase. The average crystalline size of the synthesized TiO_2 and TiO_2:Ce^{3+} particles were calculated using XRD patterns according to the Scherrer equation with FWHM of (101) peak:

$$D = \frac{(0.89 \times \lambda)}{(\beta \times \cos\ \theta)}$$

where; D is the crystalline size, β is full with half maximum of 2θ peak, λ is the wavelength of radiation, and, θ is the angle of (101) XRD peak.

Calculations revealed a decrease in the crystalline size of the TiO_2 from 15.49 to 14.19 nm, for the Ce^{3+} free and Ce^{3+} doped forms respectively, which can be assigned to the cerium addition and consequent segregation of the doping ions at grain boundaries, or, the existence of Ce–O–Ti bonds on interstitial sites and surface of the sample, which inhibit grain growth [37,38]. The peak observed in the overlapping spectrum in Fig. 1 (b) at 25.6° indicates the effect of the Ce^{3+} on the TiO_2 lattice. The slight shift and peak broadening observed in the spectrum can be attributed to the different ionic radii of the Ti^{4+} and Ce^{3+} ions [39–42]. Since the ionic radii of Ce^{3+} ions are higher than the Ti^{4+}, the replacement of the Ce^{3+} with the Ti^{4+} is difficult. Therefore, the Ti^{4+} ions can also incorporate into interstitial positions in the crystal structure. In both cases, due to the differences between the radii of these two ions, the incorporation of the Ce^{3+} ions in the crystal structure can cause some distortion in the crystal structure and these contractions cause some change in the d-spacing and lattice parameters. However, the existence of only one phase in the spectrum indicates that Ce^{3+} ions were successfully incorporated into the crystal structure of the TiO_2 [43–47] .

3.2. Composite preparation

Phosphor-based emissive composites were prepared by mixing 120 mg of PMMA in 2 mL of THF under continuous magnetic stirring. 10 mg of Phosphor and an equal mass of TiO_2 or TiO_2:Ce^{3+} were added to the vial. The obtained viscous liquid was cast on a 125 μm Mylar sheet by spin-coating technique. Thicknesses of the films were measured using Ambios Technology XP-2 Surface Profilometer and were found to be 17 ± 0.6 μm (n = 12). The films were cut to an appropriate size and placed onto the solid sample holder or diagonally located into the quartz sample cuvette of the spectrofluorometer for the spectral scans. The exact compositions of the used phosphors and additives were shown in

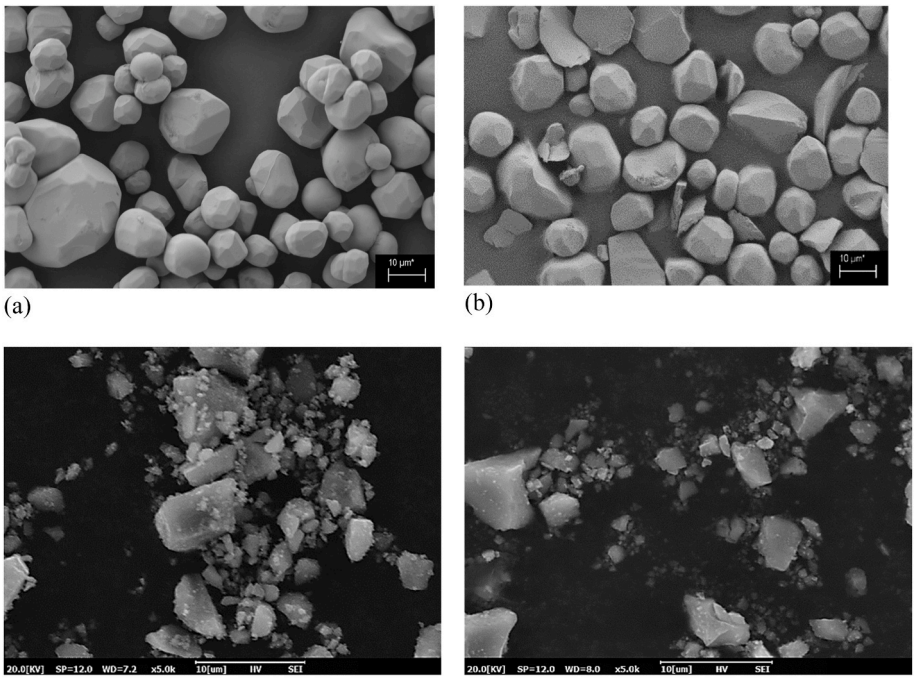


Fig. 2. SEM images of the (a) LuAG:Ce^{3+}, (b) YAG:Ce^{3+}, (c) TiO_2 and (d) TiO_2:Ce^{3+} particles.

Table 2.

3.3. Morphologies and size of the polymer-free and embedded particles

SEM images of the polymer-free LuAG: Ce^{3+}, YAG: Ce $^{3+}$, TiO_2, and TiO_2: Ce^{3+} particles are presented in Fig. 2. The phosphors; LuAG and YAG attract attention with well-shaped spherical morphology of about 15–20 μm diameters (See Fig. 2 (a) and (b)). Moreover, traces of some mechanical processes can be observed on the phosphor surfaces. Fig. 2 (c) and (d) indicate SEM photographs of the sol-gel synthesized TiO_2 and Ce^{3+}-doped TiO_2 particles which have a random particle shape with sharp corners and an average particle size of 1–2 μm.

The front surface and cross-section SEM photographs of the composites shown in Fig. 3 a-e indicate the homogeneous distribution of the luminescent particles in the PMMA matrix. As shown in earlier detailed experimental studies including NMR, photoluminescence spectra, and TEM pictograms, the PMMA provides an appropriate moiety for the phosphors in terms of dispersion as well as optical properties [34–36].

To interpret the optical interactions most accurately, particle size and zeta potential measurements were applied to the TiO_2-based particles and the results are presented in Fig. 4(a) and (b), respectively. While theTiO_2 particles are exhibiting an average particle size of 1.582 μm, diameters of the Ce^{3+} doped particles were found to be 1.451 μm. In agreement with the crystal size measurements, doping with the Ce^{3+} ions shifted the average particle size distribution towards lower dimensions (see Fig. 4 (a)). The zeta potential measurement charts of the TiO_2 particles produced by the sol-gel method can also be seen in Fig. 4 (b). Average zeta potential values were found to be −1.03 mV and −8.15 mV for the TiO_2 and, TiO_2:Ce^{3+} particles, respectively. The Ce^{3+} doping process caused a shift in the apparent zeta potential to more negative values. Both of the measured zeta potentials in the dispersant were considered stable for an efficient repulsion between the particles.

3.4. Spectral properties of the Ce^{3+} activated LuAG and YAG in the PMMA matrix

Spectral properties of the green and yellow phosphors of LuAG: Ce^{3+} and YAG: Ce^{3+} were examined when they are alone, and in the presence of the TiO_2 or TiO_2: Ce^{3+}, respectively. Fig. 5 reveals excitation and emission spectra of the LuAG and YAG and corresponding electronic transitions when excited at 450 and 466 nm, respectively. The two excitation bands centered at 344 and 450 nm in the room temperature spectrum of the LuAG corresponds to transitions of the electrons from the two lowest energy levels of the five crystal field lying in D2 symmetry (Fig. 5-I) [48–50]. Analogous photoluminescence spectra exhibited broad emission bands centered at 516 and 566 nm for the LuAG: Ce^{3+} and YAG: Ce^{3+}, respectively. The FWHM (full width at half maximum) of the phosphors were found to be 108 and 121 nm, for the LuAG and YAG. Generally, the 5d→4f emission transitions terminate on the ground 4f-level of Ce^{3+}, with positions of the Stark sublevels defined by the spin-orbit coupling [51]. In both of the phosphors, the $4f^0 5d^1$ electrons of the Ce^{3+} undergo 2D term split (2 $D_{3/2}$ and 2 $D_{5/2}$), and, the ground-state 4f1 configuration forms 2 $F_{7/2}$ and 2 $F_{5/2}$ states via spin-orbit coupling due to the different effects of the crystal field parameters of the LuAG and YAG. Therefore, the broad-band emissions observed in the phosphors can be assigned to the sum of the two overlapping sub-bands arising from the splitting of the 2 F state to the 2 $F_{5/2}$ and 2 $F_{7/2}$ states, respectively. Presence of radiative recombination of electron-hole pairs on Ce^{3+}; evidenced by electron paramagnetic resonance experiments; suggest the presence of defects in the vicinity of Ce^{3+} ions [50,52]. The Stokes' shift for the LuAG: Ce^{3+} and YAG: Ce^{3+}were found to be 66 and 100 nm, respectively which is an indication of non-radiative relaxations in the phosphors. The YAG: Ce^{3+} exhibited very similar excitation bands to the LuAG: Ce^{3+} centered at 340 and 466 nm, arising from the transitions of the Ce^{3+}. The corresponding emission maximum appeared at 566 nm (See Fig. 5. II). The larger Stokes shift (100 nm) observed for the YAG: Ce^{3+} with respect to the LuAG: Ce^{3+} (66 nm) can be attributed to room temperature phosphorescence centered at 568 nm which occurs from comparatively lower

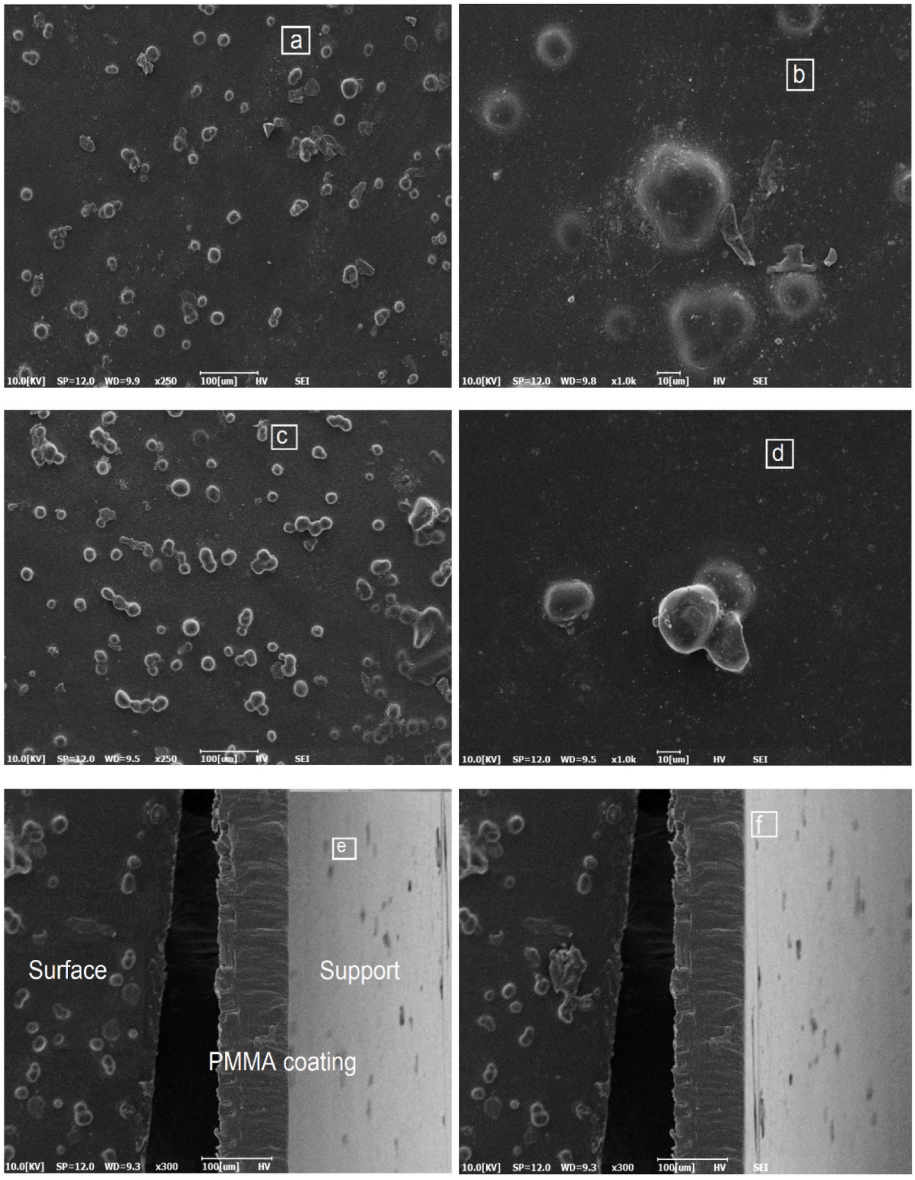


Fig. 3. SEM Photographs of the thin film films from the front surface (a) LuAG: Ce^{3+} (b) LuAG: Ce^{3+}-TiO_2: Ce^{3+}(c) YAG: Ce^{3+} and, (d) YAG: Ce^{3+}-TiO_2: Ce^{3+}, and cross-section (e and f) in the PMMA.

energy excited triplet states compared to the LuAG: Ce^{3+} [24,53]. Additionally, the covalency of the Ce^{3+} in the YAG lattice is larger than for the Ce^{3+} in the LuAG. The Ce^{3+} emission may appear between the ultraviolet and blue spectral region in the oxides, depending on the surroundings. In the presence of higher covalency and strong crystal field, the 5d orbital shifts to lower energies, resulting in emission in the yellow and even red wavelengths. Therefore, the observed longer wavelength and larger band emission of the Ce^{3+} in the YAG:Ce^{3+} at 566 nm with respect to the LuAG:Ce^{3+} (516 nm) can be assigned to the dropping of the lowest energy 5d state of the Ce^{3+} by synergistic effects of the large crystal field splitting and high covalency.

3.5. Spectral behavior of the LuAG: Ce^{3+} -TiO_2 and Ce^{3+}-doped TiO_2 blends

Following the individual tests, optical properties of the LuAG: Ce^{3+} were recorded when it is together with the Ce^{3+}-free and Ce^{3+} doped TiO_2 particles. The excitation and emission intensities of the **LuAG: Ce^{3+}-TiO_2 and - LuAG: Ce^{3+} TiO_2: Ce^{3+}** containing blends exhibited 119 and 280% enhancement in the emission intensity. The red-shift values of 32 and 52 nm were reported for the two blends, respectively.

Fig. 6 shows the gathered luminescence spectra of the additive-free LuAG: Ce^{3+} - and, -TiO_2 and TiO_2: Ce^{3+}-based composites, respectively. Potential energy transfer effects were observable in the emission spectra of the titanium dioxide-containing composites.

To reveal the potential donors and acceptors, the excitation and emission of each form were handled separately. Normalized excitation-emission spectra of the components of the blends were shown in Fig. 7 –I and, –II respectively. The shaded area, in each case, indicates the overlap region between the emission integral of the potential donor (TiO_2) and the excitation spectrum of the acceptor (LuAG: Ce^{3+}) counterparts. According to Fig. 7 –I and –II, the used additives have been effective in the enhancement of the emission intensity. Both the TiO_2 and TiO_2:Ce^{3+}; strongly absorb between 250 and 400 nm and emit at a large wavelength range extending from 400 to 500 nm covering the excitation band of the LuAG: Ce^{3+} which makes an energy transfer between these two pairs possible (See Fig. 7-I and -II). However, the co-existence of the Ce^{3+} both in the TiO_2 (TiO_2: Ce^{3+}); and phosphor at the same time resulted in an unexpected effect creating a lower intensity enhancement in the emission of the phosphor with respect to the Ce^{3+}−free TiO_2. This can be

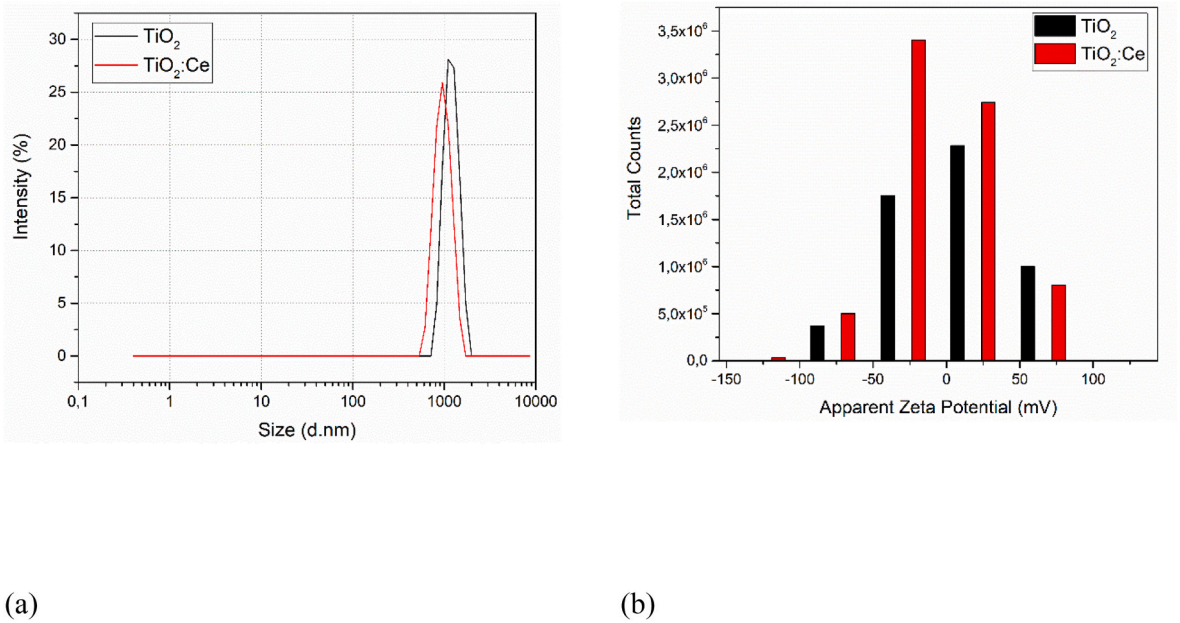


Fig. 4. (a) Particle size distribution and (b) zeta potential measurement results of the TiO_2 and TiO_2: Ce^{3+} particles.

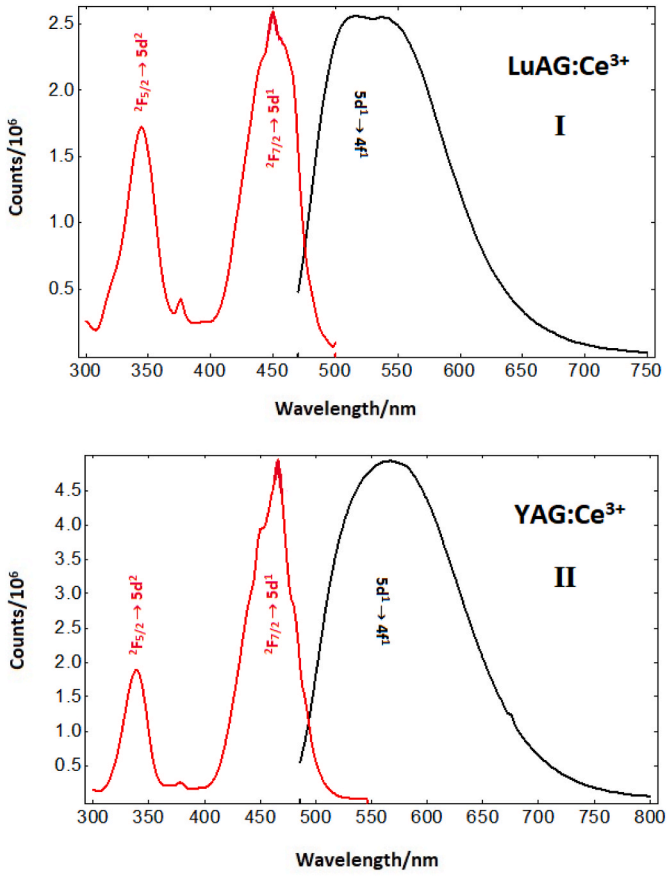


Fig. 5. Excitation and emission spectra of the green and yellow phosphors in the PMMA and corresponding electronic transitions (**I:** LuAG: Ce^{3+}; λex = 450 nm λem = 516 nm, **II:** YAG: Ce^{3+}; λex = 466 nm λem = 566 nm).

attributed to the more exact match between the emission maximum of the TiO_2 (444 nm) and the excitation maximum of the LuAG (450 nm). Despite nearly the same overlap integral for both composites, in the case

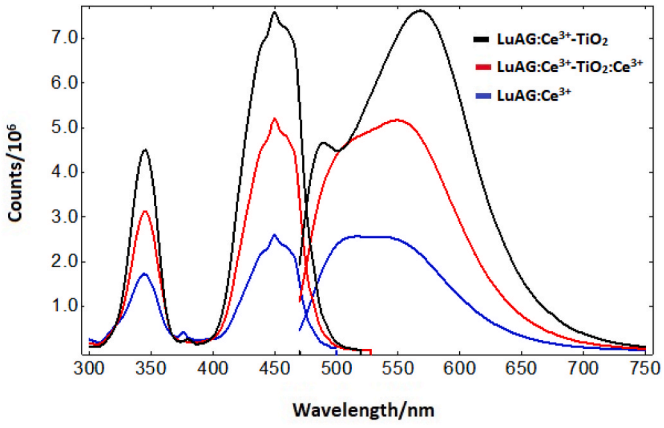


Fig. 6. Excitation-emission spectra of the additive-free LuAG: Ce^{3+} and TiO_2 or TiO_2: Ce^{3+} doped forms. Excitation has been performed at 450 nm.

of the TiO_2: Ce^{3+}; the emission maximum of the donor (422 nm) is 28 nm far from the excitation maximum of the acceptor counterpart (450 nm).

Another issue to be considered in the energy transfer is the distance between the particles as well as their morphologies. So far, the energy transfer has been studied by many researchers in detail and well explained for the solution phase. Similar research has also been performed in the solid state, utilizing the donor-acceptor pairs in the same crystal structure [54–56]. In these studies, investigators have carried out the energy transfer and approved this by experiments increasing the concentration of the acceptor species in response to the donor form within the lattice. However, the structure of the PMMA-assisted blends studied here is quite different from both, the solution phase and the crystal-based studies. The absorption and emission ability of the TiO_2 under excitation, arise from the transition of valence band electrons of the TiO_2 particles, following trapping and quenching of the photo-generated carriers by defects and, electron-hole recombination processes. Due to the superior light harvesting properties and photocatalytic efficiency, TiO_2 has specifically been investigated in terms of the charge carrier dynamics, including trap, transfer, and recombination of the photo-generated electrons and holes by using EPR, transient

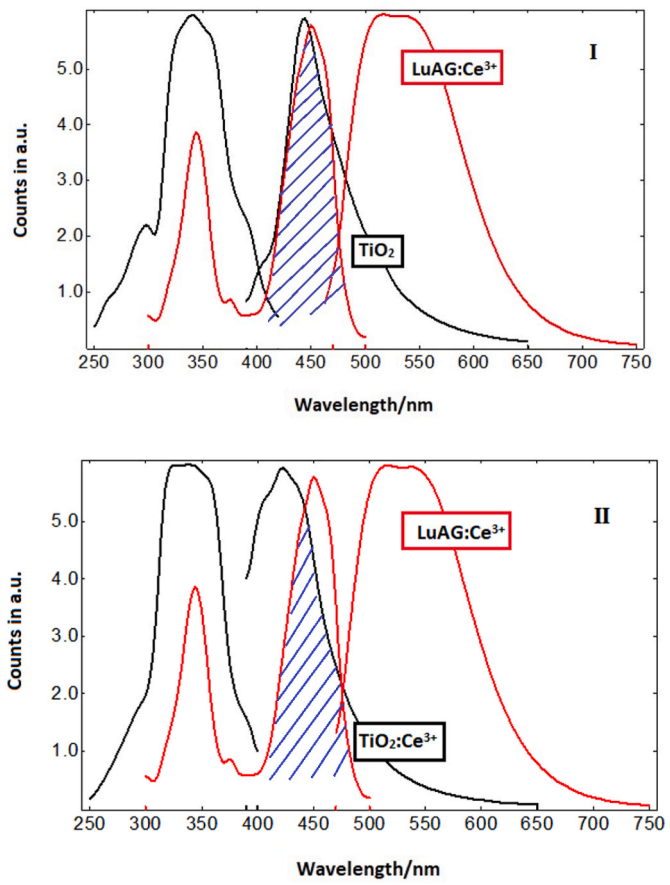


Fig. 7. I: Normalized luminescence spectra of the LuAG: Ce^{3+} and TiO_2 in the PMMA. (LuAG: Ce^{3+}; λex = 450 nm λem = 516 nm, TiO_2; λex = 342 nm λem = 444 nm) **II:** Normalized spectra of the LuAG: Ce^{3+} and TiO_2: Ce^{3+} (LuAG: Ce^{3+}; λex = 450 nm λem = 516 nm, TiO_2: Ce^{3+}; λex = 338 nm λem = 422 nm).

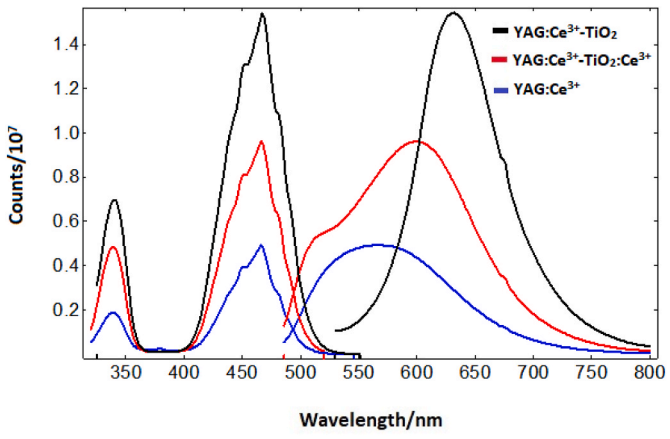


Fig. 8. Excitation-emission spectra of the additive-free YAG: Ce^{3+} and TiO_2 or TiO_2: Ce^{3+} doped forms. Excitation has been performed at 466 nm.

absorption spectroscopy, and time-resolved IR spectroscopy. These approaches provided valuable information on the relaxation and recombination behavior of photo-induced electrons or holes, respectively [57–62]. Steady-state mode photoluminescence measurements as well as time-resolved studies, on the other hand, clarified the irradiative recombination processes of the photo-generated carriers. According to the transient absorption spectroscopists, the recombination processes taking place in the TiO_2 are very sensitive to the excitation wavelength

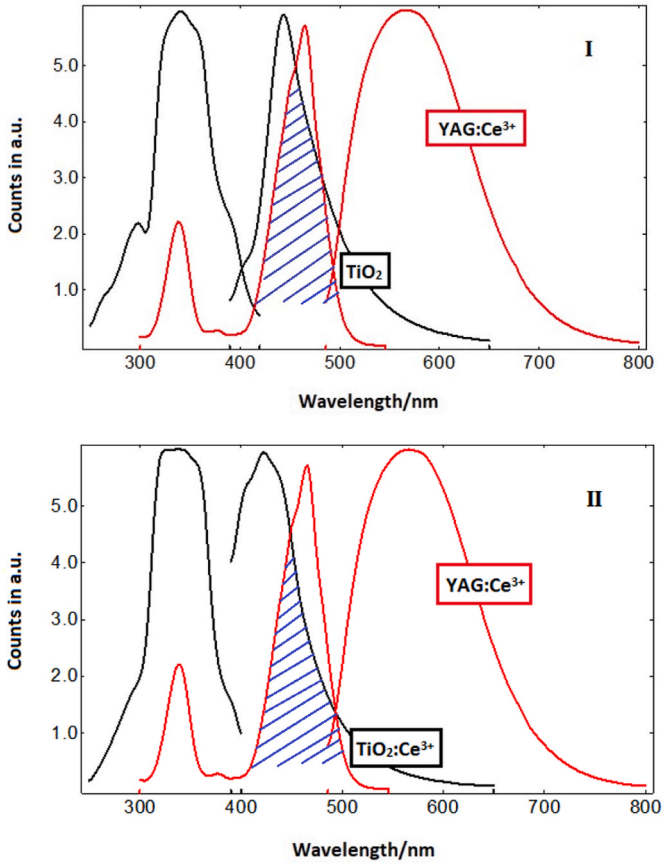


Fig. 9. I: Normalized luminescence spectra of the YAG: Ce^{3+} and TiO_2 in the PMMA. (YAG: Ce^{3+}; λex = 466 nm λem = 566 nm, TiO_2; λex = 342 nm λem = 444 nm) **II:** Normalized spectra of the LuAG: Ce^{3+} and TiO_2: Ce^{3+} (YAG: Ce^{3+}; λex = 466 nm λem = 566 nm, TiO_2: Ce^{3+}; λex = 338 nm λem = 422 nm).

[59,63–65]. Therefore, the observed enhancement in the brightness of the composites, and the light-induced interactions taking place between the phosphors and the TiO_2-based particles under excitation at 450 nm, should be evaluated in a different category other than the well-known energy transfer mechanisms observed in the solution phase from one molecule to another lying in the Förster distance, or, in the solid-state occurring between the donor-acceptor sides within the same lattice. The reason for the energy transfer lies in the fact that the TiO_2 favors light absorption and the photoexcited electrons of the TiO_2 particles may be transferred from the CB and the VB towards the phosphors creating new additional steps when they are encapsulated at a critical distance to allow this transfer.

3.6. Spectral behaviors of the YAG: Ce^{3+} -TiO_2 and Ce^{3+}-doped TiO_2 blends

Spectral response of the YAG: Ce^{3+}- TiO_2-based composites were investigated in a similar way to the LuAG: Ce^{3+} based forms. Fig. 8 indicates excitation-emission spectra of the additive-free YAG: Ce^{3+}; and, -TiO_2-based composites, upon excitation at 466 nm. While the YAG: Ce^{3+} is exhibiting a broad-band emission centered at 566 nm when blended with the TiO_2: Ce^{3+} particles, a 1.5-fold increase (140%) and 34 nm of red-shift were observed in the luminescence intensity and the emission maximum, respectively. When blended with the Ce^{3+}-free TiO_2, the enhancement in intensity and red-shift were found to be 220% and 66 nm, respectively. Figs. 8 and 9, manifest the potential energy transfer between the YAG: Ce^{3+} and the TiO_2- based additives briefly. Fig. 9 –I and –II reveal the large overlap area between the individually recorded emission integral of the TiO_2 and the TiO_2: Ce^{3+} with the

Table 3
Decay times of the polymer-free and polymer-embedded phosphors and their blends with the TiO_2 and TiO_2:Ce^{3+} in the nanosecond time scale.

Sample	λ_{max}^{ex} (nm)	λ_{max}^{ex} (nm)	χ^2		Decay time (ns)	Std. Dev. (ns)	Rel. (%)
				τ_1	29.33	1.16	15.21
LuAG:Ce^{3+} **(Polymer-free)**	450	516	1.052	τ_2	55.59	0.31	84.79
				τ_{avr}		**51.70**	
				τ_1	3.02	0.12	7.89
LuAG:Ce^{3+} **Thin Film**	450	516	1.018	τ_2	51.38	0.18	92.11
				τ_{avr}		**47.51**	
				τ_1	7.04	0.68	2.51
LuAG:Ce^{3+} - TiO_2 **Thin Film**	450	568	1.054	τ_2	55.56	0.15	97.49
				τ_{avr}		**54.35**	
				τ_1	3.45	0.16	6.84
LuAG:Ce^{3+} - TiO_2:Ce^{3+} **Thin Film**	450	548	1.124	τ_2	54.28	0.21	93.16
				τ_{avr}		**50.72**	
				τ_1	29.52	1.33	10.84
YAG:Ce^{3+} **(Polymer-free)**	466	554	1.089	τ_2	64.39	0.28	89.16
				τ_{avr}		**60.70**	
				τ_1	2.15	0.07	7.04
YAG:Ce^{3+} **Thin Film**	466	566	1.174	τ_2	61.34	0.17	92.96
				τ_{avr}		**57.20**	
YAG:Ce^{3+} - TiO_2 **Thin Film**	466	632	1.183	τ_1	66.61	0.12	100.00
				τ_{avr}		**66.61**	
				τ_1	0.82	0.03	19.19
YAG:Ce^{3+} - TiO_2:Ce^{3+} **Thin Film**	466	600	1.101	τ_2	63.14	0.15	80.81
				τ_{avr}		**51.17**	

excitation bands of the YAG: Ce^{3+}. However, further evidence relying on decay time-based measurements is necessary to explain the enhancement in the emission intensity.

3.7. Decay kinetics of the LuAG: Ce^{3+}, YAG: Ce^{3+} and their TiO_2-based blends

Decay characteristics of the Ce^{3+} activated LuAG and YAG have been investigated many times [49–51]. Most of these studies focused on the nano-scale lifetimes arising from the Ce^{3+} emission. In a few studies, however, results have been reported on both; the -nanosecond and -microsecond time-scale. Some afterglow observed in these studies indicated the role of defects in the garnets. Ogiegło et al. reported decay curves of the Ce^{3+} emission in the samples co-doped with different Tb^{3+} concentrations in a LuAG host in nano-, micro-, and millisecond time scales where the potential reasons and complexity of the microsecond time scale results have been discussed [51]. Herein we report nanosecond and microsecond time scale decays of the PMMA entrapped LuAG: Ce^{3+}, YAG: Ce^{3+}, and their blends with the Ti-based oxides, respectively. While the sub-nanosecond decay times are interpreted as the excitation of free excitons and their trapping at defect sites, those resulting from normal defects and free excitons occur on a nanosecond time scale. The presence of the deeply trapped holes manifests themselves as microsecond lifetimes. To clarify all these potential transitions, and, to understand their interactions with the TiO_2 within the matrix, we recorded short and long lifetime decay components of the samples, both; in the -nanosecond and -microsecond time scales. The nanosecond time

Table 4
Decay times of the LuAG: Ce^{3+}, YAG: Ce^{3+} and their blends with TiO_2 and TiO_2: Ce^{3+} in PMMA matrix recorded in microsecond scale.

Sample	λ_{max}^{ex} (nm)	λ_{max}^{em} (nm)	χ^2		Decay Time (μs)	Std.Dev. (μs)	Rel. (%)
				τ_1	10.25	0.12	48.62
LuAG: Ce^{3+}	450	516	1.342	τ_2	131.34	3.96	20.39
				τ_3	1122.36	30.94	30.99
				τ_{avr}		**379.70**	
				τ_1	11.99	0.14	36.88
LuAG: Ce^{3+} - TiO_2	450	568	1.265	τ_2	170.98	4.14	24.54
				τ_3	1355.72	32.51	38.59
				τ_{avr}		**561.45**	
				τ_1	12.00	0.17	35.83
LuAG: Ce^{3+} - TiO_2: Ce^{3+}	450	548	1.200	τ_2	168.98	4.95	25.80
				τ_3	1245.48	37.79	38.36
				τ_{avr}		**521.55**	
				τ_1	10.70	0.09	65.87
YAG:Ce^{3+}	466	566	1.285	τ_2	136.65	4.79	13.48
				τ_3	1155.64	35.60	20.65
				τ_{avr}		**267.50**	
				τ_1	12.05	0.12	50.76
YAG:Ce^{3+} - TiO_2	466	632	1.182	τ_2	160.13	4.78	19.28
				τ_3	1268.75	33.91	29.96
				τ_{avr}		**416.52**	
				τ_1	12.01	0.13	49.35
YAG:Ce^{3+} - TiO_2: Ce^{3+}	466	600	1.250	τ_2	160.95	5.09	20.49
				τ_3	1228.49	38.09	30.16
				τ_{avr}		**406.50**	

scale measurements were performed by using a 467 nm laser whose pulse width was significantly shorter (118.2 ps) than that of the decay times of the samples (62 and 65 ns for the LuAG and YAG- Ce^{3+}). A microsecond flash lamp was used for the measurements performed in the microsecond regime. In all cases, the intensity decays were recorded with a high-speed detection system that permits the measurement of the decay times with high accuracy. The detailed information on the photoluminescence decays of phosphors and composites are presented in Table 3 and Table 4, respectively.

3.8. Nanosecond time-scale decay time measurements

In the light of the above discussion, decay times of the PMMA embedded TiO_2 and -TiO_2:Ce^{3+}, LuAG: Ce^{3+}, YAG: Ce^{3+}, and their binary blends with the TiO_2-based oxides were recorded in nanosecond time scale (See Fig. 10). The decay curves of all samples were fitted to a bi-exponential function with the following expression.

$$I(t) = Ae^{(-t/\tau_1)} + Be^{(-t/\tau_2)}$$

where I(t) is the emission intensity as a function of time, A and B are the constants, and, τ is the decay time. The lifetimes were extracted as the time after which the intensity is dropped to 1/e of the initial value. The energy of the excitation light (2.65 eV or 467 nm) was lower than that of the band gap energy of the related host and the TiO_2-based particles (2.8 and 3.25 eV for the TiO_2 and TiO_2:Ce^{3+}). Following the literature, the polymer-free LuAG: Ce^{3+} exhibited an average decay time of 52 ns which can be assigned to the 5d−4f transition of the Ce^{3+} [50,51]. The long and short lifetime components of this decay were found to be 56 (85%) and 29 (15%) ns which indicates that the Ce^{3+} ions are located in two different sites. The bi-exponential characteristic of the decay can also be attributed to the presence of normal defects and free excitons

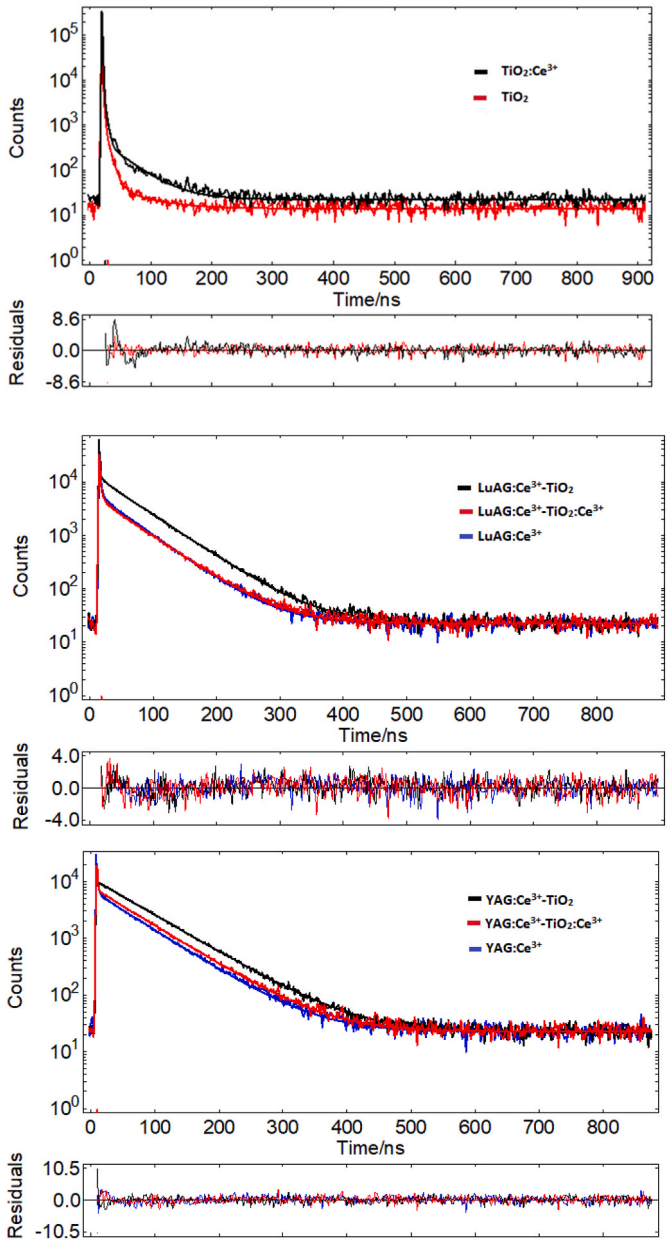


Fig. 10. Decay curves of the TiO_2-based particles, LuAG:Ce^{3+}, YAG:Ce^{3+} and their blends in PMMA matrix recorded in nanosecond time scale.

within the structure. The PMMA embedded LuAG: Ce^{3+} exhibited a slight variation both in duration and distribution of the decay components yielding 51 (92%) and 3 ns (8%) of decay times. Polymer-free and polymer encapsulated YAG: Ce^{3+} exhibited similar decays corresponding to 61 and 57 ns of average decay times, respectively (See Table 3). For both of the PMMA embedded phosphors, shortened decays were observed in comparison to their polymer-free forms. One aspect that contributes to the lifetime shortening in embedded forms may be the existence of the ester functional groups, more specifically methyl methacrylate groups in the polymer and its re-orientation and following potential light-induced interactions taking place on the polymer/-phosphor interface [64]. When blended with the TiO_2 and TiO_2: Ce^{3+} the LuAG: Ce^{3+} exhibited 54 and 51 ns average decay times, respectively. Similarly, 67 and 51 ns of average lifetimes were reported for the YAG: Ce^{3+}based blends. In the measurements performed at the nanosecond time-scale, it was determined that the TiO_2-based additives did not cause a dramatic change in the decay time values in terms of both

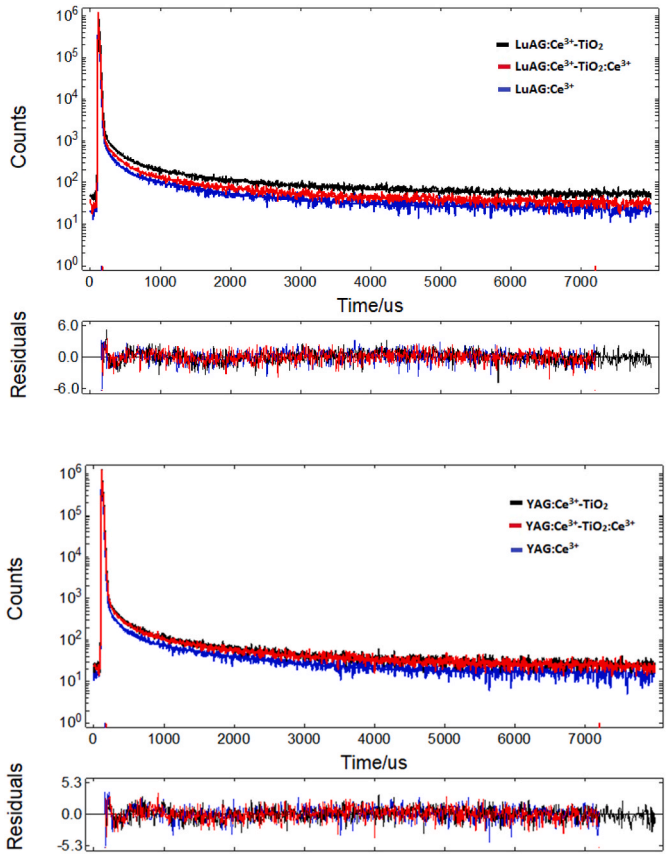


Fig. 11. Microsecond time scale decay curves of the LuAG: Ce^{3+}, YAG: Ce^{3+} and their binary blends with -TiO_2 and -TiO_2:Ce^{3+} recorded in the PMMA matrix.

duration and distribution.

3.9. Microsecond-regime decay time measurements

The decay time studies performed in the nanosecond time-scale did not present any evidence for an energy transfer or other potential events taking place between the phosphors and the additives. In contrast to the nanosecond time scale results, the decay times acquired in the microsecond time region presented interesting results that will be able to explain the reasons for the increase in emission intensity observed in the blends. The parallel improvement observed both; in the excitation and emission intensities may be relying on the microsecond and even afterglow properties of the species under investigation. Fig. 11 reveals the decay curves of the composites recorded on the microsecond time scale. Further details of the measurements for the LuAG: Ce^{3+}, YAG: Ce^{3+} and their TiO_2 and TiO_2:Ce^{3+} blends were shown in Table 4. The decay curves of the LuAG: Ce^{3+} were well fitted by three exponential decay functions when excited at 450 nm. The average decay time of the **LuAG: Ce^{3+}** in the embedded form in PMMA was **380 μs**. The distribution of the short (10 μs) mid (131 μs) and long lifetime (1122 μs) components were found to be 49, 20, and 31%, respectively. When incorporated with the TiO_2 and TiO_2:Ce^{3+}, the blends exhibited longer average decay times of **561 and 521microseconds**, respectively. Similarly, the additive-free **YAG: Ce^{3+}** exhibited three-exponential decays having short (10.7 μs, 66%) mid (137 μs, 14%), and long (1156 μs, 21%) lifetime components corresponding to an average of **267** μs. Blended forms of the YAG: Ce^{3+} however, revealed longer average decay times extending to **416 and 406** μs. Variations observed in the decay times were parallel to the enhancement reported in the emission intensities.

Table 5
Decay times of the composites prepared by the donors (TiO_2, TiO_2:Ce^{3+}) and their phosphor-blends including increasing amounts of the acceptor counterparts; LuAG:Ce^{3+} and YAG:Ce^{3+}.

Sample	Donor	Acceptor	λ_{max}^{ex} (nm)	λ_{max}^{em} (nm)	χ^2		Decay Time (μs)	Std.Dev. (μs)	Rel. (%)
						τ_1	8.19	0.12	70.86
TiO_2	TiO_2 **(5 mg)**	–	374	506	1.088	τ_2	102.55	8.54	10.38
						τ_3	782.55	50.47	18.76
						τ_{avr}	**162.80**		
						τ_1	7.95	0.10	72.35
TiO_2 - LuAG:Ce^{3+}	TiO_2 **(5 mg)**	LuAG:Ce^{3+} **(5 mg)**	374	506	1.123	τ_2	94.44	6.42	10.34
						τ_3	774.35	41.48	17.31
						τ_{avr}	**147.09**		
						τ_1	7.75	0.13	69.51
TiO_2 - LuAG:Ce^{3+}	TiO_2 **(5 mg)**	LuAG:Ce^{3+} **(10 mg)**	374	506	1.209	τ_2	61.89	4.82	10.84
						τ_3	628.52	30.14	19.65
						τ_{avr}	**135.34**		
						τ_1	8.65	0.05	83.87
TiO_2 - YAG:Ce^{3+}	TiO_2 **(5 mg)**	YAG:Ce^{3+} **(5 mg)**	374	506	1.219	τ_2	128.40	5.96	6.64
						τ_3	1020.89	46.17	9.50
						τ_{avr}	**112.73**		
						τ_1	8.72	0.07	84.81
TiO_2 - YAG:Ce^{3+}	TiO_2 **(5 mg)**	YAG:Ce^{3+} **(10 mg)**	374	506	1.171	τ_2	99.00	8.34	5.18
						τ_3	798.12	43.24	10.01
						τ_{avr}	**92.16**		
						τ_1	8.28	0.11	75.46
TiO_2:Ce^{3+}	TiO_2:Ce^{3+} **(5 mg)**	–	374	504	1.058	τ_2	122.42	10.68	9.60
						τ_3	944.48	85.99	14.94
						τ_{avr}	**157.97**		
						τ_1	8.01	0.08	76.82
TiO_2:Ce^{3+} - LuAG:Ce^{3+}	TiO_2:Ce^{3+} **(5 mg)**	LuAG:Ce^{3+} **(5 mg)**	374	504	1.102	τ_2	90.00	6.65	7.87
						τ_3	875.61	45.35	15.31
						τ_{avr}	**144.57**		
						τ_1	8.87	0.08	84.31
TiO_2:Ce^{3+} - LuAG:Ce^{3+}	TiO_2:Ce^{3+} **(5 mg)**	LuAG:Ce^{3+} **(10 mg)**	374	504	1.166	τ_2	112.96	10.79	5.86
						τ_3	870.75	71.60	9.83
						τ_{avr}	**99.33**		
						τ_1	8.06	0.10	73.19
TiO_2:Ce^{3+} - YAG:Ce^{3+}	TiO_2:Ce^{3+} **(5 mg)**	YAG:Ce^{3+} **(5 mg)**	374	504	1.165	τ_2	98.59	6.69	11.01
						τ_3	800.00	51.60	15.80
						τ_{avr}	**143.12**		
						τ_1	7.89	0.33	72.62
TiO_2:Ce^{3+} - YAG:Ce^{3+}	TiO_2:Ce^{3+} **(5 mg)**	YAG:Ce^{3+} **(10 mg)**	374	504	1.124	τ_2	51.69	14.06	8.94
						τ_3	536.94	85.75	18.45
						τ_{avr}	**106.90**		

To clarify the reasons lying behind the enhancement of the emission intensity of the phosphors in embedded form along with the TiO_2-based oxides, we focused on the classical donor-acceptor concept. Reconsidering the overlap integral between the emission spectra of TiO_2.based oxides and the excitation spectra of the phosphors, the TiO_2-based additives look like potential donors and the phosphors as the acceptors, respectively. According to the theory, if both donor and acceptor are the emitting species, energy transfer manifests itself through the quenching of donor fluorescence. A decrease in the fluorescence lifetime of the donor for the increasing concentrations of the acceptor is distinct evidence of the energy transfer. Herein, we investigated the decay behavior of the TiO_2-based donor species versus increasing concentrations of the phosphors to clearly understand the effectiveness of the TiO_2. We excited the samples at both; 450 (or 466) nm, and 374 nm, which were the optimum excitation maxima of the phosphors and, TiO_2-based oxides, respectively (See Tables 3–4, and −5). Since the TiO_2 can absorb from the UV to the visible end of the electromagnetic spectrum, it responded to both excitations. However, the emission intensity was higher in the spectrum obtained by the excitation at 374 nm. Accordingly, under the 375 nm excitation, the polymer embedded TiO_2 exhibited 163 μs of decay time. When blended with the increasing amounts of the LuAG, the TiO_2 yielded 147 and 135 μs of excited state lifetimes. In the case of the YAG-based composites, similar behavior was observed. The decay times decreased in the order of 162, 113, and 92 μs, respectively. Generally speaking, in all cases, we recorded shorter average decay times for the increasing concentrations of the YAG: Ce^{3+} and the LuAG: Ce^{3+} in comparison to the solely recorded decay times of the additives which can be concluded as evidence of an energy transfer from the TiO_2 based particles to the phosphors in the embedded form in PMMA when used in the correct concentration. Table 5 indicates the composition and detailed decay characteristics of the potential donor-acceptor pairs and their blends under the excitation of 374 nm prepared by the constant amount of the donor and increasing amounts of the acceptor, gradually. When co-existed with the phosphorus, the excited state lifetimes of the TiO_2 –based blends could not be observed properly when excited at 450 nm due to the dominance of the phosphors. In a conclusion, it is thought that the same type of energy transfer explained for the TiO_2-based particles occurs with slightly lower efficiency when the excitations are performed with blue light. In our opinion, the increases in the spectra received under 450 nm excitation can be explained in this way.

3.10. Quantum yield measurements

The external and internal quantum efficiencies (EQE and IQE) of the phosphors were given on the bases of the following equations;

$$\Phi = \frac{k_r}{k_{nr} + k_r} \quad (1)$$

where, Φ, kr and knr are the quantum yield, radiative, and nonradiative decay rate constants, respectively.

$$k_r = \Phi/\tau \quad 2$$

Table 6
External and internal quantum yield of the composites.

Sample	External Quantum Yield (%, (±1.5%, n = 3))	Internal Quantum Yield (%, (±1.5%, n = 3))
LuAG:Ce^{3+}	89.4	96.8
LuAG:Ce^{3+}-+- **TiO_2**	92.2	93.3
LuAG:Ce^{3+}- **TiO_2:Ce^{3+}**	91.4	99.1
YAG:Ce^{3+}	92.1	95.7
YAG:Ce^{3+}- **TiO_2**	96.8	97.6
YAG:Ce^{3+}- **TiO_2:Ce^{3+}**	93.7	96.9

$$k_{nr} = (1 - \Phi)/\tau \quad (3)$$

We extracted the Φ and τ parameters from the experimental results. The radiative and non-radiative decay constants (k_r and k_{nr}) were calculated from the decay times. We based on the previously published decay time data of the similar Ce^{3+} doped phosphors obtained from the nanosecond time scale measurements for comparison [66,67]. The external and internal quantum efficiencies of the studied forms were in agreement with the EQY information reported by previous investigators and were between 0.80 and 0.98 for the additive-free LuAG: Ce^{3+} and YAG: Ce^{3+} based samples. In paralell to the intensity-based measurements, we observed a brief enhancement in the external quantum yield from 89.37 to 92.19% (EQY) for the LuAG: Ce^{3+}**- TiO_2**+based composite with respect to the -LuAG: Ce^{3+} only (See Table 6). The **-TiO_2:Ce^{3+}** blends of the LuAG: Ce^{3+} yielded 91.4% EQY. Similarly, when blended with the $^{+}$**- TiO_2** and **-TiO_2:Ce^{3+}**, the YAG: Ce^{3+}based samples yielded higher EQY (96.8 and 93.7%) compared to the individual form of the phosphor (92.1%).

The internal quantum efficiency information reflecting the ratio of the number of photons emitted to the number of photons absorbed by the sample is also given in Table 6. Interestingly, the difference between the EQY and IQY was small for the - **TiO_2** blends of both phosphors, which can be attributed to the less efficiency loss due to the structural properties of the utilized material. The enhancement observed in the EQY of the blended forms is related to the particle diameter of the TiO2-based additives since the particles scatter electromagnetic radiation with a wavelength that is twice the particle diameter. Therefore, excitation light with a wavelength of 466 nm can only be scattered most strongly by particles of 233 nm diameter. Due to the chosen particle size (1.6 μm) of the additive, in our case, scattering-related losses will not be subjective for a large wavelength range including blue light.

4. Conclusion

In this study, photoluminescence of the green and yellow phosphors of lutetium aluminum (LuAG: Ce^{3+}), and, yttrium aluminum garnets (YAG: Ce^{3+}), and their blends with the Ti- oxides have been investigated in detail by steady-state and decay time measurements.

When the phosphors were embedded in the PMMA matrix along with the TiO_2 and Ce^{3+} activated TiO_2 particles; displayed an extraordinary increase in the excitation and emission intensities and shorter excited lifetimes with respect to their additive-free forms.

When excited at 450 nm, the LuAG: Ce^{3+}-TiO2-based blend exhibited 280% enhancement in intensity and 32 nm of red-shift in the emission maximum. Similarly, when yttrium aluminum garnet (YAG: Ce^{3+}) was incorporated with the TiO_2, the emission intensity exhibited 220% improvement. A 66 nm of red shift in the emission maximum was accompanied by an increase in brightness. In the case of the Ce^{3+} activated additives (TiO_2:Ce^{3+}), the enhancement in the emission intensities was reported as 119 and 140% for the LuAG: Ce^{3+} and YAG: Ce^{3+}, respectively. Decay times of the phosphors and their blends were measured carefully in the nanosecond and microsecond regions of the time scale. The microsecond time regime studies presented some evidence regarding an energy transfer from the Ti-based oxides to the phosphors. The energy transfer was more effective in the case of Ce^{3+}-free additives. The excitation ability of the TiO_2-based phosphor blends by the blue wavelengths, and, consequent very efficient red-shifted emission performance may be promising for a lot of applications including WLEDs and screen technologies.

CRediT authorship contribution statement

Beyza Yildirim: Experimental part, Data curation, data processing. **Ozgur Yasin Keskin:** Experimental part, Data curation, data processing. **Ramazan Dalmis:** Experimental part, Data curation, data processing, Conceptualization. **Isil Birlik:** Writing – original draft, preparation, Conceptualization. **Funda Ak Azem:** Writing – original draft, preparation, Conceptualization. **Kadriye Ertekin:** Supervision, Methodology, Writing – original draft, Conceptualization.

Declaration of competing interest

The authors declare that they have no known competing financial interests or personal relationships that could have appeared to influence the work reported in this paper.

Data availability

Data will be made available on request.

Acknowledgment

This research was funded by the Scientific Research Funds of Dokuz Eylul University (project number: 2020 KB FEN.026 We also would like to thank “Turkey, Council of Higher Education Ph.D. scholarship program (YOK 100/2000)”.

Appendix A. Supplementary data

Supplementary data to this article can be found online at https://doi.org/10.1016/j.optmat.2022.112905.

References

[1] A. Birkel, K.A. Denault, N.C. George, C.E. Doll, B. Hery, A.A. Mikhailovsky, C. S. Birkel, B.C. Hong, R. Seshadri, Rapid microwave preparation of highly efficient Ce3+-substituted garnet phosphors for solid state white lighting, Chem. Mater. 24 (2012) 8–1204.
[2] W.S. Silveira, A.J.S. Silva, P.A.M. do Nascimento, I.D. Carvalho, M.V.D. Rezende, Improving the luminescence properties of YAG:Ce3+ phosphors by co-doping Sr2+ ions, Optik (2021) 231.
[3] H. Ding, Z.H. Liu, P. Hu, Y.F. Liu, P. Sun, Z.H. Luo, X.P. Chen, H.C. Jiang, J. Jiang, High efficiency green-emitting LuAG:Ce ceramic phosphors for laser diode lighting, Adv. Opt. Mater. 9 (2021).
[4] A. Cantarano, A. Ibanez, G. Dantelle, Garnet-type nanophosphors for white LED lighting, Front Mater 7 (2020).
[5] C.J. Cozzan, S.P. DenBaars, R. Seshadri, Ce: Yag/Al2o3 Composites for Laser-Excited Solid-State White Lighting, Google Patents, 2019.
[6] J.H. Song, H. BoYong, Lighting Apparatus and Lighting System Including the Same, Google Patents, 2021.
[7] K.T. Kim, B.G. Min, Light Emitting Diode Package, Google Patents, 2010.
[8] S. Seo, N. Ohsawa, Light-emitting Element, Display Device, Electronic Device, and Lighting Device, Google Patents, 2020.
[9] S. Senbonmatsu, Self Light Emitting Display Device, Google Patents, 2006.
[10] S. Yamazaki, T. Konuma, J. Koyama, K. Inukai, M. Mizukami, Display Device Using Light-Emitting Element, Google Patents, 2011.
[11] A.A. Setlur, A.M. Srivastava, H.A. Comanzo, Red Phosphor for LED Based Lighting, Google Patents, 2008.
[12] T.F. Soules, W.W. Beers, A.M. Srivastava, L.M. Levinson, A.R. Duggal, Light Emitting Device with Phosphor Composition, Google Patents, 2001.
[13] X. Cao, S.C. Sun, B. Lu, Y. Liu, R. Ma, H.Q. Cao, H.Z. Ma, H.X. Huang, Spectral photoluminescence properties of YAG: Ce, R (R: Gd3+, Pr3+, Gd3+ and Pr3+) transparent fluorescent thin film prepared by pulse laser deposition, J. Lumin. 223 (2020).
[14] B. Wen, D.F. Zhang, N. Zhang, J.K. Feng, B. Jiang, F.S. Pan, Y.H. Zhang, L. Yang, Effect of grain size on the luminescent properties of Ce3+ doped Y3Al5O12 ceramic phosphor plates, Ceram. Int. 46 (2020) 10452–10456.

[15] C. Gu, X.J. Wang, C.H. Zhang, Q.Q. Zhu, Effect of boron carbide (B4C) on luminescent efficiency and thermal stability of Y3Al5O12:Ce3+ phosphors, J. Lumin. (2020) 226.
[16] H. Ali, M.A. Khedr, Energy transfer between Ce and Sm co-doped YAG nanocrystals for white light emitting devices, Results Phys. 12 (2019) 1777–1782.
[17] X.W. He, Y.B. Ren, C.X. Hu, B. Ma, H. Chen, S.S. Huang, H.Y. Hao, T.T. Qi, X.F. Liu, R.H. Yu, Clarifying the effect of local structure of Ce3+ and Eu3+ on photoluminescence of YAG:Ce,Eu nanophosphors, J. Alloys Compd. (2020) 822.
[18] J. Xu, J. Ueda, K. Kuroishi, S. Tanabe, Fabrication of Ce3+-Cr3+ co-doped yttrium aluminium gallium garnet transparent ceramic phosphors with super long persistent luminescence, Scripta Mater. 102 (2015) 47–50.
[19] Y.J. Song, Q.Q. Liu, N. Zong, Z.M. Wang, D.F. Cui, S.J. Zhang, Y. Bo, Q.J. Peng, Spectroscopic properties and energy transfer in Nd3+/Yb3+ co-doped yttrium aluminum garnet, Laser Phys. 31 (2021).
[20] M. Skruodiene, A. Katelnikovas, L. Vasylechko, R. Skaudzius, Tb3+ to Cr3+ energy transfer in a co-doped Y3Al5O12 host, J. Lumin. 208 (2019) 327–333.
[21] C.Y. Zhao, Y.T. Duan, H. Lin, D.W. Zhang, R.J. Hong, C.X. Tao, Z.X. Han, S. M. Zhou, Synthesis and luminescence properties of color-tunable Ce, Mn co-doped LuAG transparent ceramics by sintering under atmospheric pressure, Ceram. Int. 47 (2021) 9156–9163.
[22] S.P. Liu, X.Q. Feng, Z.W. Zhou, M. Nikl, Y. Shi, Y.B. Pan, Effect of Mg2+ co-doping on the scintillation performance of LuAG: Ce ceramics, Phys Status Solidi-R 8 (2014) 105–109.
[23] M. Sugiyama, T. Yanagida, Y. Fujimoto, Comparative study of Tm-doped and Tm-Sc co-doped Lu3Al5O12 scintillator, Radiat. Meas. 71 (2014) 153–157.
[24] J.M. Ogieglo, A. Zych, K.V. Ivanovskikh, T. Justel, C.R. Ronda, A. Meijerink, Luminescence and energy transfer in Lu3Al5O12 scintillators Co-doped with Ce3+ and Tb3+, J. Phys. Chem. A 116 (2012) 8464–8474.
[25] W.Q. Ma, B.X. Jiang, S.L. Chen, X.Q. Feng, Q.Q. Zhu, L. Zhang, K. Sreebunpeng, A fast lutetium aluminum garnet scintillation ceramic with Ce3+ and Ca2+ co-dopants, J. Lumin. (2019) 216.
[26] M. Kucera, M. Nikl, P. Prusa, J.A. Mares, K. Nitsch, M. Hanus, Z. Onderisinova, R. Kucerkova, Growth and emission properties of Sc, Pr, and Ce co-doped Lu3Al5O12 epitaxial layers for scintillators, J. Cryst. Growth 318 (2011) 813–819.
[27] P. Hu, Y.F. Liu, P. Sun, Q. Yao, Z.H. Liu, Z.H. Luo, K.F. Chao, H.C.A. Jiang, J. Jiang, Tunable YAG:Ce3+ ceramic phosphors for white laser-diode lighting i transmissive/reflective models, Mater. Res. Bull. 140 (2021).
[28] B. Yan, Y. Wei, W. Wang, M.Q. Fu, G.G. Li, Red-tunable LuAG garnet phosphors via Eu3+-> Mn4+ energy transfer for optical thermometry sensor application, Inorg. Chem. Front. 8 (2021) 746–757.
[29] J. Huang, Y.R. Ni, Y.L. Ma, Y.B. Li, Z.X. Sun, X.Y. Zhu, R. Wang, T. Li, X.Q. Xi, G. C. Huang, T.Y. Zhou, M. Li, H.D. Ren, L. Zhang, H. Chen, Composite structure Cr: YAG/Ce:YAG and (Ce,Cr):YAG/Ce:YAG transparent ceramics with high color rendering index for white LEDs/LDs, Ceram. Int. 47 (2021) 11415–11422.
[30] K. Park, T. Kim, Y. Yu, K. Seo, J. Kim, Y/Gd-free yellow Lu3Al5O12:Ce3+ phosphor for white LEDs, J. Lumin. 173 (2016) 159–164.
[31] B. Yildirim, O.Y. Keskin, S. Oguzlar, I. Birlik, F.A. Azem, K. Ertekin, Manipulation of brightness and decay kinetics of LuAG: Ce3+ and YAG: Ce3+ by simple metal oxides in polymeric matrices, Opt Laser. Technol. 142 (2021), 107226.
[32] B. Yildirim, R. Dalmis, K. Ertekin, I. Birlik, F.A. Azem, Enhancing optical properties of Lu3Al5O12:Ce3+ by cost-effective silica-based photonic crystals, J. Mater. Sci. Mater. Electron. 31 (2020) 10267–10278.
[33] B. Yildirim, K. Ertekin, S. Demirci, S. Gultekin, Boosting optical performance of polymer embedded phosphors using iodine-free and iodine-decorated sol-gel synthesized alpha-Fe2O3, Opt. Mater. 95 (2019), 109238.
[34] F. Armetta, M.A. Sibeko, A.S. Luyt, D.F. Chillura Martino, A. Spinella, M. L. Saladino, Influence of the Ce: YAG amount on structure and optical properties of Ce:YAG-PMMA composites for white LED, Zeitschrift fur Phys. Chemie 230 (9) (2016) 1219–1231.
[35] M.L. Saladino, A. Zanotto, D. Chillura Martino, A. Spinella, G. Nasillo, E. Caponetti, Ce:YAG nanoparticles embedded in a PMMA matrix: preparation and characterization, Langmuir 26 (16) (2010) 13442–13449.
[36] M.L. Saladino, D. Chillura Martino, M.A. Floriano, D. Hreniak, L. Marciniak, W. Strek, E. Caponetti, Ce:Y3Al5O12–Poly(methyl methacrylate) composite for white-light-emitting diodes, J. Phys. Chem. C 118 (2014) 9107–9113.
[37] G. Xiao, X. Huang, X.P. Liao, B. Shi, One-pot facile synthesis of cerium-doped TiO2 mesoporous nanofibers using collagen fiber as the biotemplate and its application in visible light photocatalysis, J. Phys. Chem. C 117 (2013) 9739–9746.
[38] M. Nasir, S. Bagwasi, Y.C. Jiao, F. Chen, B.Z. Tian, J.L. Zhang, Characterization and activity of the Ce and N co-doped TiO2 prepared through hydrothermal method, Chem. Eng. J. 236 (2014) 388–397.
[39] O.Y. Keskin, R. Dalmis, I. Birlik, N.F.A. Azem, Comparison of the effect of non-metal and rare-earth element doping on structural and optical properties of CuO/TiO2 one-dimensional photonic crystals, J. Alloys Compd. (2020) 817.
[40] N.N. Yan, Z.Q. Zhu, J. Zhang, Z.Y. Zhao, Q.J. Liu, Preparation and properties of ce-doped TiO2 photocatalyst, Mater. Res. Bull. 47 (2012) 1869–1873.
[41] Y. Liu, P.F. Fang, Y.L. Cheng, Y.P. Gao, F.T. Chen, Z. Liu, Y.Q. Dai, Study on enhanced photocatalytic performance of cerium doped TiO2-based nanosheets, Chem. Eng. J. 219 (2013) 478–485.
[42] T. Yu, X. Tan, L. Zhao, Y.X. Yin, P. Chen, J. Wei, Characterization, activity and kinetics of a visible light driven photocatalyst: cerium and nitrogen co-doped TiO2 nanoparticles, Chem. Eng. J. 157 (2010) 86–92.
[43] Y.L. Cheng, M. Zhang, G. Yao, L. Yang, J.J. Tao, Z.Z. Gong, G. He, Z.Q. Sun, Band gap manipulation of cerium doping TiO2 nanopowders by hydrothermal method, J. Alloys Compd. 662 (2016) 179–184.
[44] S. Oguzlar, M.Z. Ongun, O.Y. Keskin, T.K. Delice, F.A. Azem, I. Birlik, K. Ertekin, Investigation of spectral interactions between a SrAl2O4:Eu2+, Dy3+ phosphor and nano-scale TiO2, J. Fluoresc. 30 (2020) 839–847.
[45] K. Moradi, C. Depecker, J. Corset, Diffuse-Reflectance Infrared Fourier-Transform Spectroscopy - a Comparison with Theory of the Diffusion of Nonabsorbing Powders, vol. 1993, P Soc Photo-Opt Ins, 2009, pp. 324–325.
[46] C.W. Huang, B.J. Lin, H.Y. Lin, C.H. Huang, F.Y. Shih, W.H. Wang, C.Y. Liu, H. C. Chui, Observation of strain effect on the suspended graphene by polarized Raman spectroscopy, Nanoscale Res. Lett. 7 (2012).
[47] R. Borja-Urby, L.A. Diaz-Torres, I. Garcia-Martinez, D. Bahena-Uribe, G. Casillas, A. Ponce, M. Jose-Yacaman, Crystalline and narrow band gap semiconductor BaZrO3: Bi-Si synthesized by microwave-hydrothermal synthesis, Catal. Today 250 (2015) 95–101.
[48] A.A. Setlur, A.M. Srivastava, On the relationship between emission color and Ce3+ concentration in garnet phosphors, Opt. Mater. 29 (2007) 1647–1652.
[49] J.L. Wu, G. Gundiah, A.K. Cheetham, Structure-property correlations in Ce-doped garnet phosphors for use in solid state lighting, Chem. Phys. Lett. 441 (2007) 250–254.
[50] J.Q. Liu, X.J. Wang, T.T. Xuan, C.B. Wang, H.L. Li, Z. Sun, Lu-3(Al,Si)(5)(O,N)(12): Ce3+ phosphors with broad emission band and high thermal stability for white LEDs, J. Lumin. 158 (2015) 322–327.
[51] D.N. Petrov, B.M. Angelov, Spin - orbit coupling and quasi - nephelauxetic effect in Ce3+, Physica B (2020) 579.
[52] W. Ahn, Y.J. Kim, Effects of flux on the synthesis and the luminescence of Lu3Al5O12:Ce3+ phosphors, Sci Adv Mater 8 (2016) 904–908.
[53] M. Nikl, A. Vedda, M. Fasoli, I. Fontana, V.V. Laguta, E. Mihokova, J. Pejchal, J. Rosa, K. Nejezchleb, Shallow traps and radiative recombination processes in Lu3Al5O12 : Ce single crystal scintillator, Phys Rev B (2007) 76.
[54] J.C.A. Santos, E.P. Silva, D.V. Sampaio, D.C. Silva, N.R.S. Souza, C. Kucera, J. Ballato, R.S. Silva, Effect of the Ce3+ concentration on laser-sintered YAG ceramics for white LEDs applications, J Eur Ceram Soc 40 (2020) 3673–3678.
[55] S.P. Liu, X.Q. Feng, J.A. Mares, V. Babin, C. Hu, H.M. Kou, C. D'Ambrosio, J. Li, Y. B. Pan, M. Nikl, Effect of Li+ ions co-doping on luminescence, scintillation properties and defects characteristics of LuAG:Ce ceramics, Opt Mater 64 (2017) 245–249.
[56] M. Borlaf, M. Frankowska, W.W. Kubiak, T. Graule, Strong photoluminescence emission at low dopant amount in YAG:Ce and YAG:Eu phosphors, Mater Res Bull 100 (2018) 413–419.
[57] J.T. Carneiro, T.J. Savenije, J.A. Moulijn, G. Mul, Toward a physically sound structure-activity relationship of TiO2-based photocatalysts, J Phys Chem C 114 (2010) 327–332.
[58] S. Ikeda, N. Sugiyama, S. Murakami, H. Kominami, Y. Kera, H. Noguchi, K. Uosaki, T. Torimoto, B. Ohtani, Quantitative analysis of defective sites in titanium(IV) oxide photocatalyst powders, Phys Chem Chem Phys 5 (2003) 778–783.
[59] Y. Tamaki, A. Furube, M. Murai, K. Hara, R. Katoh, M. Tachiya, Direct observation of reactive trapped holes in TiO2 undergoing photocatalytic oxidation of adsorbed alcohols: evaluation of the reaction rates and yields, J Am Chem Soc 128 (2006) 416–417.
[60] S. Tojo, T. Tachikawa, M. Fujitsuka, T. Majima, Direct observation of one-electron oxidation processes of aromatic sulfides in TiO2 colloidal solution by laser flash photolysis, Phys Chem Chem Phys 6 (2004) 960–964.
[61] A. Furube, T. Asahi, H. Masuhara, H. Yamashita, M. Anpo, Charge carrier dynamics of standard TiO2 catalysts revealed by femtosecond diffuse reflectance spectroscopy, J Phys Chem B 103 (1999) 3120–3127.
[62] A. Yamakata, T. Ishibashi, H. Onishi, Electron- and hole-capture reactions on Pt/TiO2 photocatalyst exposed to methanol vapor studied with time-resolved infrared absorption spectroscopy, J Phys Chem B 106 (2002) 9122–9125.
[63] Y. Tamaki, A. Furube, M. Murai, K. Hara, R. Katoh, M. Tachiya, Dynamics of efficient electron-hole separation in TiO2 nanoparticles revealed by femtosecond transient absorption spectroscopy under the weak-excitation condition, Phys Chem Chem Phys 9 (2007) 1453–1460.
[64] H. Zhao, Q.L. Zhang, Y.X. Weng, Deep surface trap filling by photoinduced carriers and interparticle electron transport observed in TiO2 nanocrystalline film with time-resolved visible and Mid-IR transient spectroscopies, J Phys Chem C 111 (2007) 3762–3769.
[65] R. Katoh, M. Murai, A. Furube, Electron-hole recombination in the bulk of a rutile TiO2 single crystal studied by sub-nanosecond transient absorption spectroscopy, Chem Phys Lett 461 (2008) 238–241.
[66] P. Gorrotxategi, M. Consonni, A. Gasse, Optical efficiency characterization of LED phosphors using a double integrating sphere system, J. Solid State Light (2015), https://doi.org/10.1186/s40539-014-0020-7.
[67] J.R. Silva, L.H.C. Andrade, S.M. Lima, Y. Guyot, N. Giannini, M. Sheik-Bahae, Investigation of allowed and forbidden electronic transitions in rare earth doped materials for laser cooling application by thermal lens spectroscopy, Opt. Mater. (Amst). (2019), https://doi.org/10.1016/j.optmat.2019.109195.